

COLUMBIDAE UNIVERSITY

FINAL YEAR PROJECT

**Pigeons love doves**

*John Birdwatch*

supervised by

Dr. Mark BROWN

June 11, 2016

## **Copyright**

## **Committee Approval Page**

## Abstract

# Contents

<b>1</b>	<b>Introduction</b>	<b>1</b>
<b>2</b>	<b>Background</b>	<b>2</b>
2.1	Dune Pattern Studies . . . . .	2
2.2	Image Processing . . . . .	4
2.2.1	Filtering . . . . .	4
2.2.2	Illumination Normalization . . . . .	4
2.2.3	Edge and Line Detection . . . . .	5
2.2.4	Edge Linking . . . . .	7
2.3	Pattern Recognition . . . . .	8
2.3.1	Perceptual Grouping . . . . .	8
2.3.2	Watershed Segmentation . . . . .	8
2.4	Automated Feature Detection . . . . .	9
2.5	Automated Dune Detection . . . . .	11
<b>3</b>	<b>Methodology</b>	<b>12</b>
3.1	Machine Learning Approach . . . . .	12
3.1.1	Image Preprocessing . . . . .	12
3.1.2	Dominant Orientation Determination . . . . .	14
3.1.3	Crest-line Candidate Detection . . . . .	18
<b>4</b>	<b>Results</b>	<b>20</b>
4.1	Study Areas . . . . .	20
4.1.1	Terrestrial Dataset . . . . .	20
4.1.2	Mars Dataset . . . . .	24



## List of Figures

1	Results of unnormalized (red) and normalized (green) histograms of gradients ( $N = 18$ ). The histogram contains two major peaks, but the crest-line is the weaker of the two peaks. (a) Edges which belong to the dominant orientation which are invalid crest-lines. (b) With normalization, the true crest-lines now have the higher overall magnitude. (c) The 18 bin histogram of gradients with and without normalization. . . . .	16
2	. . . . .	19
3	Terrestrial dataset of six regions with respective labeled ground truth: (3a) Kala-hari (Namibia), (3b) Namib (Namibia), (3c) Simpson (Australia), (3d) Skeleton Coast (Namibia), (3e) Winnemucca Dune Complex (USA), and (3f) White Sands (USA) . . . . .	22
4	Ganges chasma Mars dataset from [4] which includes (4a) 16 regions extracted, (4b) sample image from region 1 with corresponding labeled ground truth . . .	26

## List of Tables

# 1 Introduction

This is the introduction

## 2 Background

### 2.1 Dune Pattern Studies

In [6], an explanation of how dune-field patterns emerge and addresses the degree of complexity from the standpoint of self-organizing system. Dune patterns are classified into two basic categories: simple or complex. According to this paper, a simple pattern is defined as having a single pattern type. Complex patterns are said to potentially have multiple spatially superimposed pattern types. Simple patterns trend towards a better ordering, so long as the wind regime remains constant. Changes in the trend of wind pattern will cause reorientation. Complex patterns can then be interpreted as the superposition of many generations of wind regimes.

Complexity can be measured using pattern analysis, measuring parameters such as the crest length, orientation, spacing, defect density, and other properties. These properties would be very useful information to extract for the dune detection. Finding crest-lines can help us identify the patterns, extracting meaningful data such as junctions, terminations, mergers, linking, and other interesting processes explained in [6].

In later work, [33] studied the dune field pattern formations on the north polar region of Mars. These dunes are thought to be mostly inactive, with relative no movement over a period of 4 to 15 Martian years. The reason this region is interesting is because there are two nearly orthogonal crest-line orientations present in the region. This complex system of superposition of multiple patterns in this example showcase a set of *primary* and *secondary* crest-lines which would be valuable data to automatically segment. The *primary* dunes are the largest-scale dunes, extend over the entire length of the image set, and contain many *Y* junctions, an indication of well-organized linear dunes. In contrast, *secondary* dunes are rounded, have least defined features, and are perpendicular to the main primary crest-lines.

Other interesting features are the so-called *Slipfaces*. These typically appear along the *primary* crest-lines, in areas of intersection with the *primary* and *secondary* crest-lines. Another feature are the *Wind Ripples*. The ripples are present on the surface of most dunes with the exception of *slipfaces*. To detect these types of features, a higher resolution image is required, as those types of features are very small compared to the scale of the *primary* and *secondary* dunes. *Interdune Areas* are features specific to the area studied in [33], have a polygonal shape, and are indicative of ice.

The rest of the paper describes an in depth statistical analysis of the features to compute the flow fields and understand the geomorphic relationships which are present in the area. The paper [33] provides a lot of interesting and valuable information which can be used to understand the application of automatic dune detection. If these features can be extracted, it would be interesting to see if we can do a similar statistical analysis based on the results presented. The next step would be to retrieve the HiRISE dataset and their data or ground truth to compare.

In the most recent work, [31] study the aeolian dune-fields at different scales. Scale is an important factor to consider because aeolian dune-fields patterns can vary over a wide range of scales, both spatially and temporally. Being able to measure the change of scale over time is important in order to investigate the environmental conditions of the studied region. Aeolian dunes are developed typically in transitions from sand patches, to proto-dunes, to dunes, to dune-field patterns. Complex dune patterns are usually a juxtaposition of simple dune patterns at multiple scales. To summarize, being able to detect the crest-lines and other types of features at multiple scales is invaluable.

In other related work, [5] studied the migration of submarine sand dunes. The dataset used in this paper includes digital terrain models (DTMs) retrieved from high-density multibeam echosounders (MBES) taken of submarine sand dunes along the coast of New Brunswick. In

order to measure the migration of these types of dunes, the motion was measured by simply subtracting the DTMs from sequences over time. The implementation uses a simple cross-correlation to find similarities from one set to the next. From the correlation matches found, the migration vector can be computed. The migration data processing can extract the flow fields of the dunes.

## **2.2 Image Processing**

### **2.2.1 Filtering**

There are many common filtering approaches used in image processing and computer vision applications. In this application, satellite images of sand dunes may include various amounts of noise. In order to improve the dune detection algorithms, the goal of filtering is to filter out the noise while preserving or enhancing the necessary features such as the crest-line edges.

In [2], the bilateral filter is proposed, which allows flat noisy regions to be filtered while preserving strong edges. Bilateral filtering is a simple non-iterative algorithm for filtering out noise.

### **2.2.2 Illumination Normalization**

Illumination normalization is a process in which the image illumination is made to be more evenly distributed across the image, to make the illumination invariant in conditions of varying lighting. This processing is most commonly used in face detection or recognition applications.

In [41], a Gaussian illumination model is used to stretch the contrasts of darker areas. The process involves using a Quadtree method to divide the image into sub regions to find dark areas. The areas that meet these requirements are processed with the Gaussian illumination model to brighten them up, which evens out the illumination. Applying this normalization significantly

improves performance of face recognition.

In a similar approach [8], the authors use a modified retinex algorithm to restore poorly illuminated areas of an image. According to Lambertian reflectance theory, images consist of two components, reflectance and illumination. If an image contains a set of small scale features, and large scale features, and illumination is only applied to the large-scale set, then the small scale features can be preserved. In this approach, the normalization is applied to small-scale and large-scale features independently. The Single Scale Retinex process is applied to the image to separate the reflectance (small scale) and illumination (large scale). After, images are thresholded and histogram equalization is applied, which spreads out intensity values of darker areas of the image.

In a remote sensing application, [12], illumination normalization in the gradient domain and using singular value equalization. According to the authors, the gradient domain image enhancement process can compress the dynamic range of images, increase contrast, and enhance fine details in darker regions. The goal of singular value equalization is to make all images in a specific set to have similar mean intensity value. Some images may have a lower or higher mean intensity. By using SVE, the pixels can be processed to achieve a mean closer to the target intensity, therefore normalizing illumination across a set of images. The drawback of this method is that multiple images of the same or similar scenes are required.

### **2.2.3 Edge and Line Detection**

The Canny edge detector is a well known and used method to retrieve important edge features from an image. In [25], enhancement to the method is proposed by analyzing the responses of detection at two scales. The benefits of this technique are better localization in images with larger amounts of noise, at the cost of a slightly lower detection rate. Overall the performance

of the Canny operator is improved by using multiple scales.

The Canny detector is further improved in [40] for a runway detection application for unmanned aerial vehicles. The main contribution of this paper is the use the Canny operator combined with a mean filter, and using the Hough Transform to track runways. The advantages of the mean filtering is that it filters out noise, preserves edges (better than a traditional Gaussian filter), and makes the image less fuzzy. To solve the problem of the dual threshold of the Canny operator, the proposed method is to compute the thresholds dynamically based on averages.

In [39], an improved implementation of the popular Canny edge detector is proposed. According to the authors, the traditional Canny algorithm suffers from two main problems: the gradient calculation is sensitive to noise and the use of the fixed double threshold may not be suitable for images with high gradient variability. The main flaw in the gradient calculation has to do with the inequality of the edge detection in darker versus brighter regions. For the parameter selection of the double threshold, the paper propose choosing the high and low thresholds from the computed mean and standard deviation of the gradient magnitudes.

A line detection and image enhancement has been proposed in [7], for a digital image restoration of heritage art application. The images worked with have been deteriorated over time, and contain many cracks, faint lines, and broken stroke. The goal of this is to remove unwanted edges, and enhance the desired edges. The approach is implemented in three basic steps: Initial line detection with non-maxima suppression, true line detection using anisotropic refinement, and noise reduction.

The initial step is to perform correlation convolving the image with some sort of edge detecting mask, rotated at different orientations, and retrieving the maximum response for the orientation for each pixel. The paper claims this produces a sharper and more reliable edge map, which is then filtered using non-maxima suppression. This process preserves strong lines

while removing texture lines. The image is binarized to remove all remaining weak edges, and only allowing strong edges to remain. The smoothing is applied to the original based on the processing done, smoothing out weak edges, while not smoothing strong true edges.

In a similar approach, [35] use rotating edge detection kernels and fuse the responses from the operations. What determines what an edge is a location and a direction, as a non-edge point such as a flat area or noise, which has no specific direction. Following this principle, the response in one direction should be higher than in the other directions. For a non-edge, the responses in each of the directions are similar. Therefore computing the mean and standard deviation of each of the kernel responses can help resolve edge versus non edge pixels. The results obtained from this process shows promising results when applied to noisy images. The approach proposed in [35] has definite potential for improved edge detection applied to dune crest-line detection. It also has potential for improvement of the method itself.

An interesting alternative to the classical Hough transform is presented in [14] in an application inspection or maintenance of underwater cable components. The paper discusses image processing techniques to extract linear features in cluttered and noisy images. After applying some anisotropic filtering to remove high frequency noise, edges and lines are detected on the sonar based images. To detect potential linear features, they use a Phase Congruency detector. The Hough transform is then used to find linear features, and a criteria is determined to reject false positives and preserve true positives.

#### **2.2.4 Edge Linking**

In [42], an edge linking approach is proposed which uses local neighborhood, using geodesic distance (as opposed to the common Euclidean distance measure) between edge candidates. When calculating the direction of edge end points, typically eight directions are used, which

introduces error. To address this [42] define a windows size based on the maximum allowable edge gap, and fit a line to the edges, which allows a full range of directions to be accounted for. The geodesic distance measurement is not only based on euclidean distance but also on intensity values of the image, which reportedly gives better results.

## 2.3 Pattern Recognition

### 2.3.1 Perceptual Grouping

In [9], a tensor voting approach is used to perform perceptual grouping on noisy data. The approach extends the standard tensor voting using Bayesian probabilities. The Bayesian framework has added benefits of reducing the learning variance of the perceptual grouping task. Another contribution of this paper is the use of a 2nd order tensor and two types of polarity vectors to handle both outliers and inlier noise. The approach also is able to process all types of geometric structures. For probabilistic tensor voting, the voting procedure uses random vector with a given standard deviation. It uses three layers of voting: sparse ball vote, sparse stick vote, and revised stick vote, where the goal is to change the positions of each token based on a random vector.

### 2.3.2 Watershed Segmentation

The Watershed Transform is a well know algorithm for segmenting meaningful regions from an image. The main benefit of the watershed technique as opposed to method, such as edge-based detection, is that the watershed produces closed boundaries, which allows contours to be detected. An overview of the Watershed algorithm is presented in [29].

In [26], segmentation is achieved using the watershed transform from texture gradients. The texture gradients are retrieved using various wavelet transforms.

Similarly, in [36], an approach to texture segmentation is proposed. When applied to textures, the watershed algorithm tends to over-segment a texture into small homogeneous sub-texture regions. Therefore, a texture can be determined to be set of texture segments. The texture sub-regions can be merged using a clustering algorithm. A wavelet transform is used to characterize the irregular shaped segment regions, which are used to cluster similar groups of sub-textures.

Another approach used in the Watershed algorithm is based on markers. The desired regions to segment can be extracted using some known feature which gets marked on the image. In [34], this concept is applied to a fingerprint pore extraction application. Marker based segmentation has been shown to be robust for segmentations problems where the objects are closed contours with boundaries being ridges. In this application, the watershed transform is applied to the gradient image of the fingerprints, and the regional minimas are computed to obtain the markers, then compute the watershed transform based on the markers.

In [20], the watershed segmentation is applied to a breast tumor detection application.

## 2.4 Automated Feature Detection

In [37], a semi-automated method for extracting roads from aerial or satellite images is proposed. The purpose of this paper is to localize roads from higher resolution images, using some form of segmentation. The proposed method is semi-automated because a user must provide an initial seed point, onto which a region growing algorithm is applied to extract the road.

A level set method is applied to evolve the boundary of the road region, which can better handle noise and multiple road mergers. The boundary for the desired region is based on a speed function, which is designed based on uniformity, texture, and contrast properties. Once the regions have been extracted, the centerlines of the roads are estimated using a skeletonization

procedure, with junction analysis to ensure that intersections are properly handled.

In [3], linear features of internal waves are extracted using a technique called *Multiscale Retinex*(MSR) feature extraction. Although the problem set in [3] is different, there appears to be significant overlap and comparison between dune crest-line detection and oceanic internal wave detection. The oceanic internal waves are typically generated from many sources such as tidal currents, ocean frontal boundaries, and other atmospheric conditions. The MSR is an image processing technique that provides consistency and dynamic range compression across an image with poor contrast. The paper discusses the use both the Wavelet Transform Modulus Maxima (WTMM) and the Canny edge detector, which turned out to have superior performance.

There has been some work done in automated dune detection. In [21], a supervised learning approach is used, training classifiers such as Support Vector Machine and Random Forests to detect dune structures on Mars. The method proposed in this paper is to classify small (40 by 40 pixels) cells in a quantized image grid. In each cells features are computed based on the image gradients, using both phase and magnitude. In order to classify a cell as either a dune or not a dune, the features of both the cell and the cell's neighboring cells are used. The features extracted are then used to train the machine learning method, which is used to then predict if a cell is a dune.

Although this type of method has typically shown very good results, there are a few drawbacks with using supervised learning approaches. These types of methods usually require a fairly large labeled dataset which may not always be available. Anytime a dataset is constructed for this purpose, it is important to provide a large number of examples of different types of dunes, in order to get a robust representation of the problem set. In [21], 230 labeled images were used to train and test the method, and have a decent representation of various dune types. Another drawback of this approach is the use of cells, for which fixed-sized cells may not be scale invariant.

ant. Also, quantizing an image into larger cells will affect localization accuracy of the dunes. If the application requires higher localization accuracy, this type of supervised learning approach may not be suitable.

## 2.5 Automated Dune Detection

In [23], an automated extraction of dune features is proposed. In this approach, the authors claim that the Canny edge detector provided poor results, and the sobel operator generated more consistent results. The gradient magnitude of the Sobel operator is used to threshold out the weaker edges. The use of a histogram to compute the orientations of the gradients was found to have a bimodal distribution, with one of the modes being the dune edges. Dune candidates are determined based on their gradient magnitude which filter out weaker candidates unless they are near strong candidates.

## 3 Methodology

### 3.1 Machine Learning Approach

In this study, many different approaches were attempted and compared to extract meaningful features from the images and compute the appropriate morphological properties of the dune fields. The approach presented in this paper can be summarized as a five stage process:

1. Image Preprocessing
2. Dominant Orientation Determination
3. Crest-line Candidate Detection
4. Validation
5. Metrics Calculations

#### 3.1.1 Image Preprocessing

The pre-processing stage is an important step to normalize and de-noise the input data. Image processing is typically a low level process which attempts to improve image quality, normalize illumination, or remove unnecessary information from the image. This type of processing will in turn improve higher level feature extraction.

The first step is to insure that the images have roughly the same scale. To enforce scale normalization, the datasets scales were manually selected for appropriate crest-line detection application, and the image resolutions were resized to roughly 1000 pixel in width. The appropriate resolution is chosen based on a few factors:

- Source resolution: The selected resolution is limited by the original image's resolution.

No extra information can be gained from increasing the source image's resolution.

- Processing time: Higher resolution images require much more processing time overall which could be a limitation in a certain application.
- Scale selection: If the application's domain is found in a higher scale space, a higher resolution may not necessarily be required.

In this application, the goal is to detect the major crest-line, which is a higher scale domain, which means a higher resolution image is not a necessity. Note that some of the parameter selection in these processes are dependent on the resolution and scale of the images. In future work, dominant scale of the crest-lines could be determined automatically to improve the robustness of the algorithms.

The next step in the process is to convert the images to gray scale. The images in the terrestrial, and Ganges datasets (described in section 4.1.1 and 4.1.2) are color images by default. Although color processing of these images has not extensively been tested as part of this study, it is arguable whether using color information would improve the detection results. By converting the images to gray scale, an added benefit of normalizing the images across many region is implicitly enforced. Finally, the conversion process turns the three channel image into a single channel image which improves overall processing performance.

The final preprocessing step is to improve the image quality with low-pass filters. Many of the algorithms in this method rely on gradient information. Therefore, to extract the meaningful gradients, removing the highest frequencies (which in typically are responsible for noise), while preserving the lower scale or more desirable gradients. Two main popular filters are utilized. The median filter, introduced in [1], is applied first to remove grain and salt and pepper noise while preserving important edges. In some cases, median filtering also helps remove some smaller scale objects such as bushes, trees, rocks, and other features which are indistinguishable from satellite images. Following is the standard Gaussian filter which removes the remaining

high frequency noisy signals from the image.

An important aspect to note is the size of the filter masks, which is heavily dependent on the resolution of the input image. We found that in most cases, for images around 1000 pixels in width, a *sigma* value of approximately 1.5 and mask size of 7 by 7 was sufficient for this application. Once the image has been preprocessed, the gradients can be computed and saved for future use. Gradients can be computed by taking the first derivative of the image, using the popular Sobel operator.

An optional additional step is to apply histogram equalization to the image [28]. Poorly illuminated or low contrast images greatly benefit from histogram equalization, because it stretches the contrast of the image in a consistent way. Using this process has shown to improve the overall results in many cases.

### **3.1.2 Dominant Orientation Determination**

Computing the dominant orientation of the dune field is an important step in the process. The dominant orientation is the gradient direction of the crest-lines to be detected. This process can help determine the average orientation of the dune field as well.

An important point to make is that this process could be optional if the dominant orientation is known a priori. Working with a dataset where the values are known improves the overall results of detection and enables skipping of this step. In cases where this information is unknown, or unavailable, automated dominant orientation determination is a potential solution.

Typically, there exists a gradient peak at the crest-line peak of the dunes (although this may not always be the case for less pronounced dunes). The direction of the gradient should agree with the overall dominant orientation of the dune field. Computing the dominant orientation of the field can be challenging in many cases because dunes typically have two major orientations,

which are opposite directions. This phenomenon is clearly illustrated in Figure 1. The true crest-line peak, where the sunny side meets the shaded side is one gradient (fig. 1b). At the foot of the dune, where the shaded returns to light, a second gradient will be present, whom has an opposite direction (fig. 1a).

To remedy this issue, using histograms of gradient directions can be used to determine the true orientation. Histograms have been used for many processes and applications including [22, 24, 30]. Quantizing the space allows us to split edges according to their orientation, where each bin in the histogram represents an edge orientation. Each bin then covers an angle of  $\frac{2\pi}{N}$  radians, where  $N$  is the number of bins. Each bin of the histogram is weighed by the magnitude of edges. Once the histogram is constructed, peaks in the magnitude will help determine the dominant orientation ( $\Phi$ ) of the dune crest-lines. The approach poses two main problems:

1. Determining  $N$ : In practice, a larger value for  $N$  has shown to provide finer grain resolution which improves dominant orientation determination. In Figure 1 a value of  $N = 18$  is used.
2. Multiple Peaks: Often, images may have multiple peaks in the histogram, but only one of the peaks should represent the true dominant orientation of crest-lines.
3. Global Solution: The computed dominant orientation is global to the image, which may not be optimal in cases of complex dune structures. A better solution would be to compute the dominant orientation in a local area of the image, to account for local shifts in orientation.

One assumption made is that the bin with the largest value represents the orientation of the crest-line edges. Although this assumption holds for many cases, it is not always the case. The Skeleton Coast test image provides a good example of this case in Figure 1. In this particular

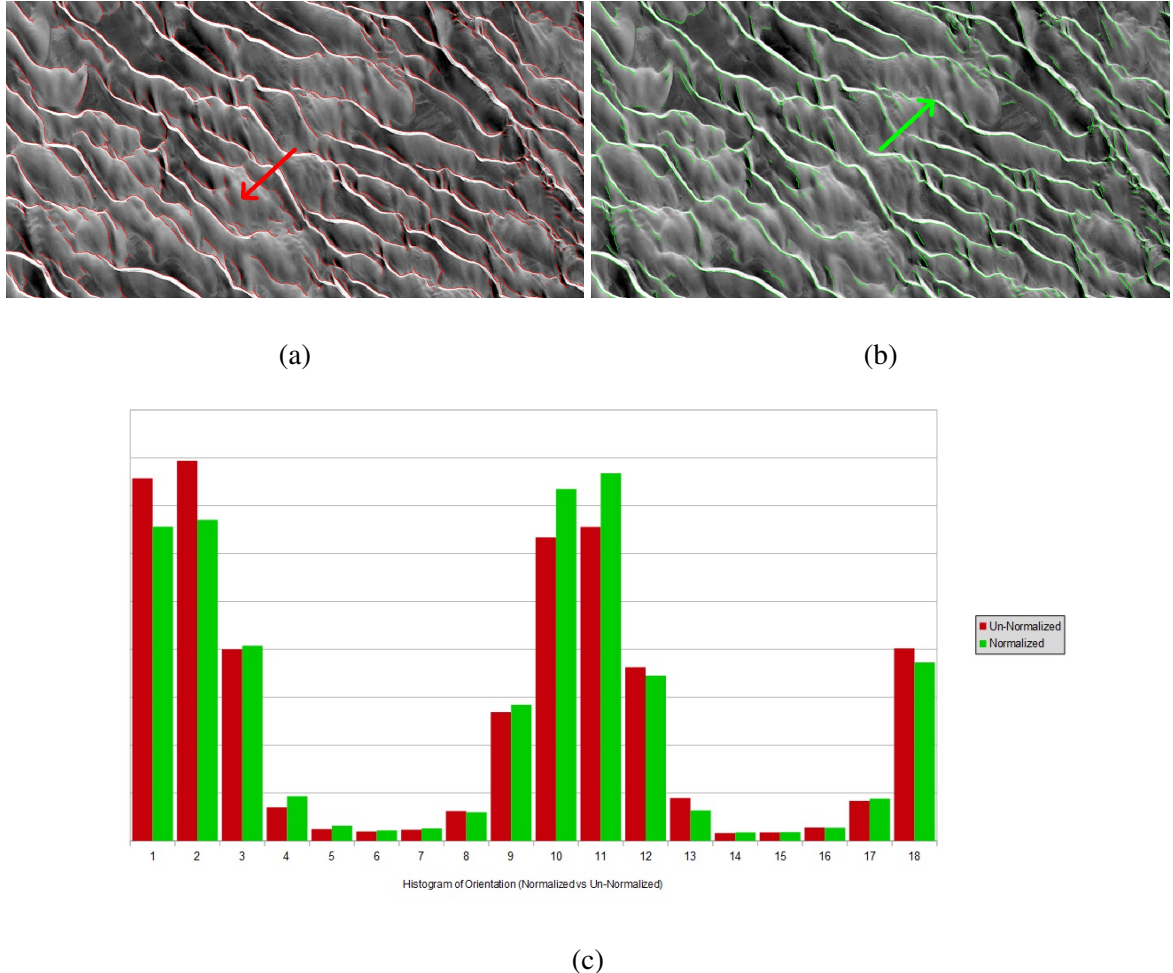


Figure 1: Results of unnormalized (red) and normalized (green) histograms of gradients ( $N = 18$ ). The histogram contains two major peaks, but the crest-line is the weaker of the two peaks. (a) Edges which belong to the dominant orientation which are invalid crest-lines. (b) With normalization, the true crest-lines now have the higher overall magnitude. (c) The 18 bin histogram of gradients with and without normalization.

case, there are two major peaks in the histogram, where the stronger is not the part of the crest-line edge group, and the weaker one is. Choosing the higher peak will cause invalid crest-lines to be chosen. In order to determine which peak best represents the crest-line edge group, some normalization can be applied. The normalization process begins by computing the mean vector of the gradients from the edge image as follows:

$$\hat{\mu} \langle \bar{x}, \bar{y} \rangle = \left\langle \frac{\sum_{i=0}^P \delta_{x_i}}{P}, \frac{\sum_{i=0}^P \delta_{y_i}}{P} \right\rangle$$

where  $P$  is the total number of detected edges from the Canny edge detector,  $\delta_{x_i}$  and  $\delta_{y_i}$  are the  $x$  and  $y$  gradient component of the  $i^{\text{th}}$  point. The mean orientation is computed from the mean vector as:

$$\bar{\theta}_\mu = \arctan \left( \frac{\mu_{\bar{y}}}{\mu_{\bar{x}}} \right)$$

The gradients are then normalized by simply subtracting the mean vector from each gradient:

$$\dot{\delta}(x_i, y_i) = (\delta_{x_i} - \mu_{\bar{x}}, \delta_{y_i} - \mu_{\bar{y}})$$

The normalized orientation  $\dot{\theta}_i$  can be computed:

$$\dot{\theta}_i = \arctan \left( \frac{\dot{\delta}_{y_i}}{\dot{\delta}_{x_i}} \right)$$

To determine which bin the  $i^{\text{th}}$  edge point belongs to, we simply calculate  $\left[ \frac{\dot{\theta}_i * N}{2\pi} - 0.5 \right]$ , and increment that bin by the magnitude of the normalized gradient by  $\sqrt{\dot{\delta}_{x_i}^2 + \dot{\delta}_{y_i}^2}$ . In essence, this normalization process removes the uneven skew of the gradients in the overall image. Removing this skew allows true crest-line edges to be fairly compared with other stronger edges. As shown in Figure 1, the normalization process softens the stronger dominant edge and enhances the true

crest-line edges. This process enables true crest-lines to be accurately determined in images where the valleys of dunes are sharp and contain strong edges.

Once the histogram is computed and normalized, the dominant orientation vector  $\hat{\theta}_{dom}$  is determined by averaging the gradients belonging to the histogram bin with the highest value. With the dominant orientation knowledge acquired, candidate crest-line dunes can be detected.

### 3.1.3 Crest-line Candidate Detection

The goal of the initial candidate detection step is to find as many of the true crest-lines as possible. For optimal results, candidate detections should span as much of the crest-line as possible and ideally be a single contiguous segment. These constraints help improve the overall accuracy and compute the geomorphological properties of the dune fields.

The candidate detection process can be summarized in four steps:

1. Compute the gradient orientation image relative to the dominant orientation.
2. Threshold the gradient orientation image to preserve all pixels which agree with the dominant orientation.
3. Find the contours of the thresholded regions of the gradient orientation image.
4. Shift the contours to the nearest gradient magnitude peak.

The relative gradient orientation image maps the gradient directions relative to the computed dominant orientation. This can be achieved by taking the dot product of the normalized gradient vectors, with the normalized dominant orientation vector at each pixel location on the image, as shown below.

$$R_{\theta_{ij}} = \hat{\delta}_{ij} \cdot \hat{\theta}_{dom}$$

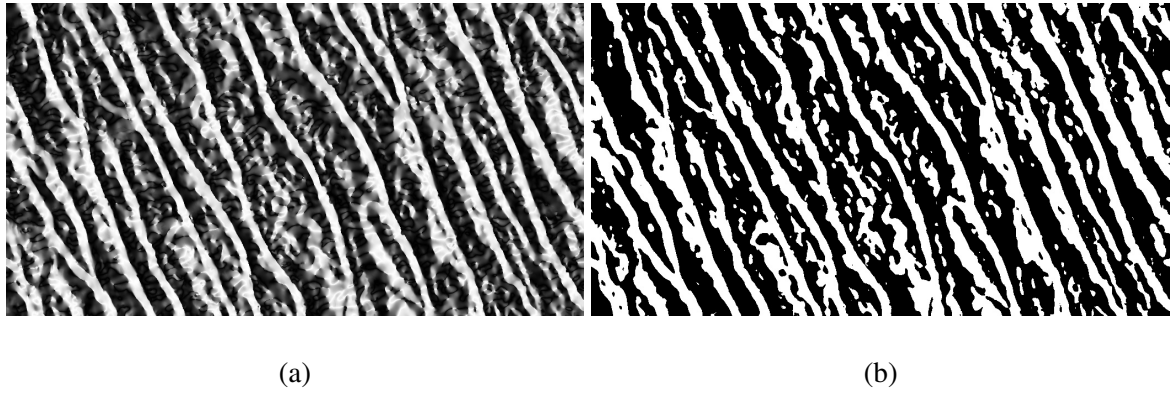


Figure 2

In essence, the resulting image  $R_\theta$  displays maps the gradient direction vectors to a single value with a range of values from  $-1$  to  $+1$ . A brighter pixel then *agrees* with the dominant orientation while dark pixels *disagrees* with it. The resulting transformation is shown in Figure 2.

The benefit of this transformation is that due to the nature of the domain problem, this produces bright regions around dune crest-lines. Another benefit is that it much less sensitive to weaker

## 4 Results

### 4.1 Study Areas

As part of this research project, two datasets were used in order to prove the robustness of this method. The datasets include a wide range of dune types with varying morphological properties.

The data provided in each set are satellite images of dune field regions available through Google Earth and NASA datasets. Included with the images is the ground truth which has been manually labeled by experts in the research field. The ground truth consists of crest-lines for each positive dune detection.

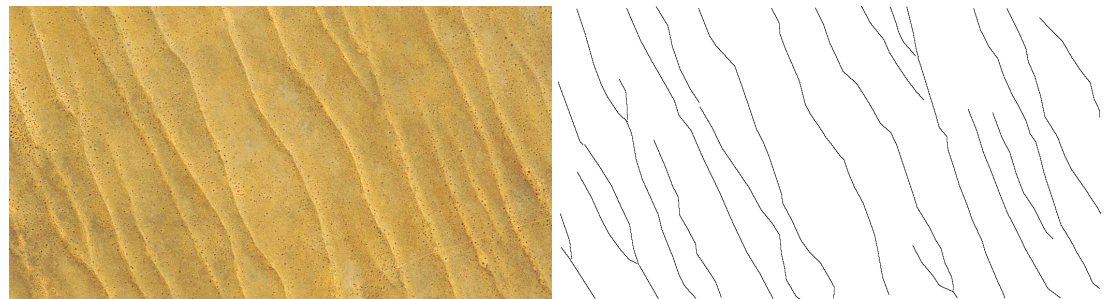
In each case, the scales of the satellite images were chosen such that the inter-dune distance appeared roughly normalized across the entire dataset. Scale selection of the images is important process for even comparison of the methods for different regions. The images are resized to an appropriate resolution for processing and even across the entire dataset.

The method described in this paper was tested on two distinct datasets: an terrestrial dataset which includes dune fields of various regions on Earth, along with the dataset provided in [4] which is located on Mars in the Ganges crater region. The same method was applied on both datasets.

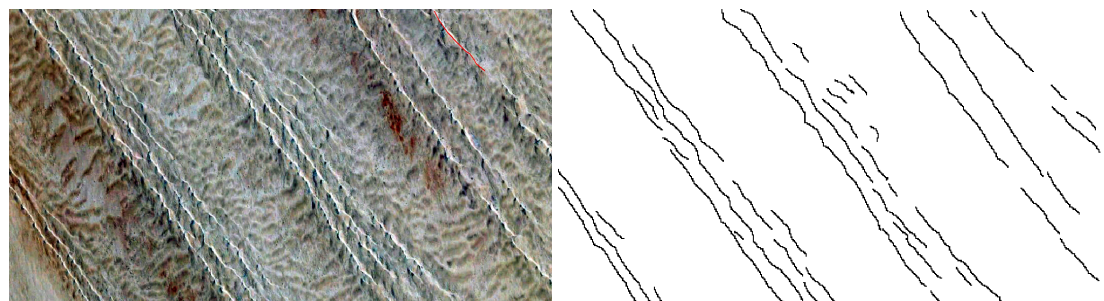
#### 4.1.1 Terrestrial Dataset

The first dataset is a small sample of a dozen satellite images from six separate desert regions on Earth (shown in Figure 3). Included are the Kalahari, Namib and Skeleton Coast sand sea regions in Namibia ([10]). Also represented in this dataset are the Simpson dune field in Australia, the Winnemucca Dune Complex in Nevada, and the White Sands National Monument. A wide range of landform types are contained within each of these regions which provides a

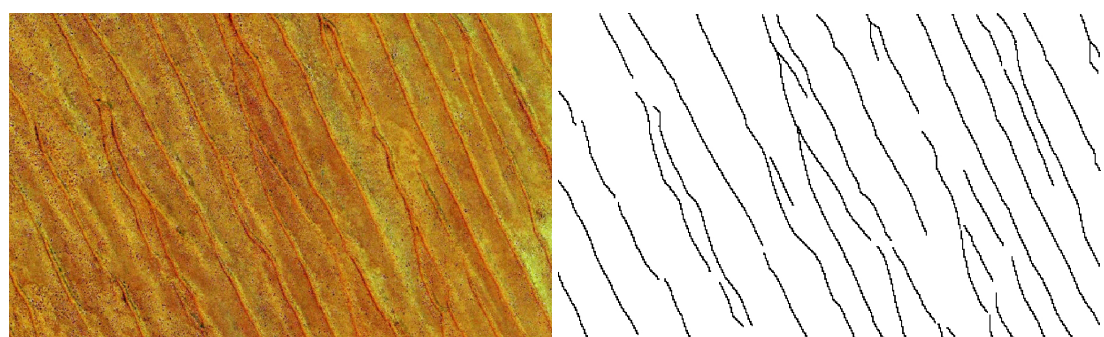
broad study for an automated crest-line detection method.



(a)



(b)



(c)

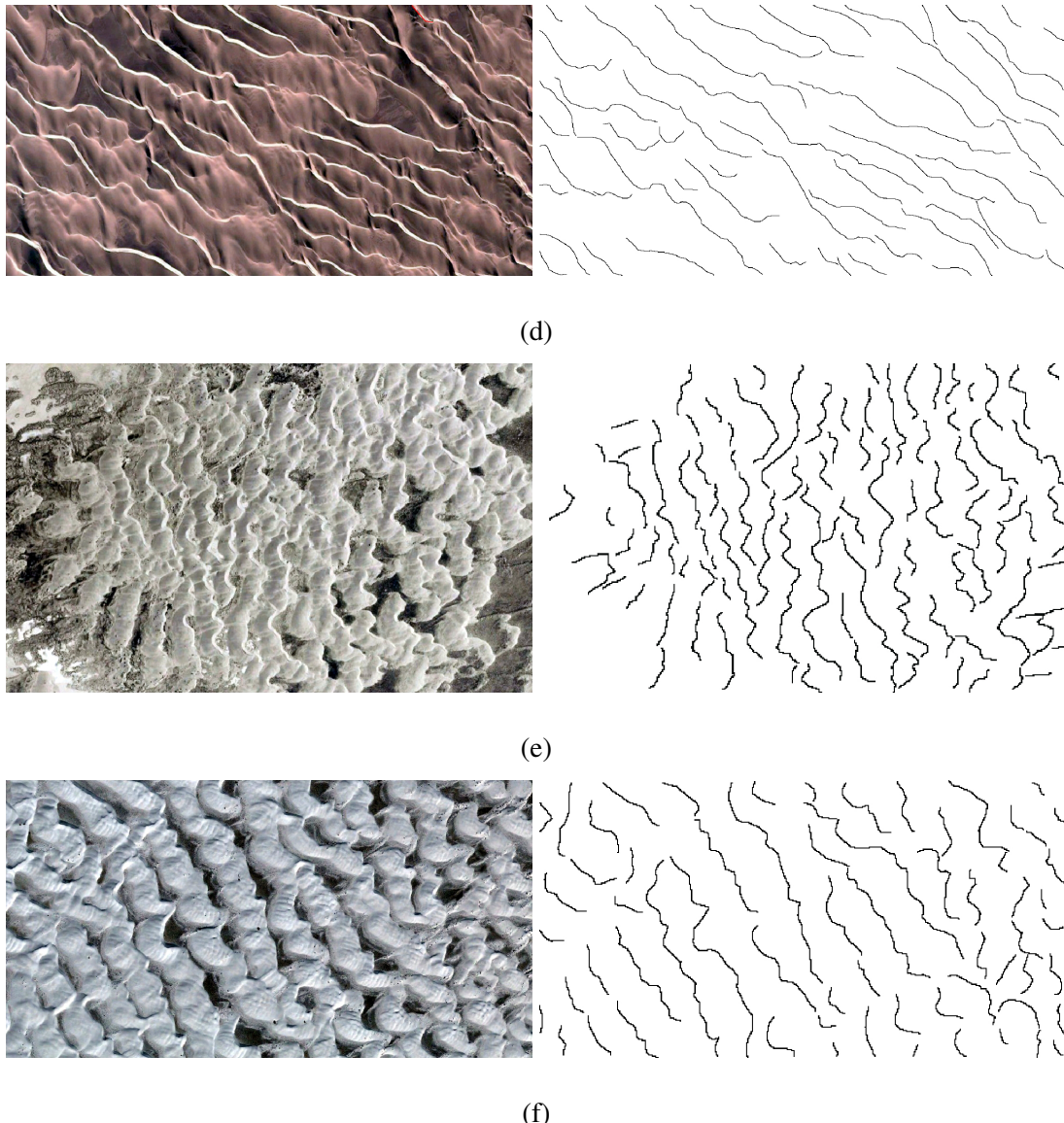


Figure 3: Terrestrial dataset of six regions with respective labeled ground truth: (3a) Kalahari (Namibia), (3b) Namib (Namibia), (3c) Simpson (Australia), (3d) Skeleton Coast (Namibia), (3e) Winnemucca Dune Complex (USA), and (3f) White Sands (USA)

The Kalahari (fig. 3a)sands span from the southeastern region of Namibia to South Africa. The region is a 100-200 km wide and is composed of mostly fixed dunes [19]. Most of the area is comprised of simple linear form dunes, although some small areas contain some compound linear dunes as well. Unlike other desert regions, the Kalahari contains areas which are well vegetated. On average, the dunes range from 2m to 15m in height, with a 150m to 250m

width, and spaced from 200m to 240m. These measurements may be useful for determining the reliability of our metric calculations.

The Namib Sand Sea (fig. 3b) region spans approximately 34,000 km of the Altantic coast of Namibia, contains some of the largest and oldest sand dunes in the world according to [11]. High energy unimodal, bimodal and complex wind regimes create interesting dune field patterns in the Namib Sand Sea region of Namibia [18]. These wind patterns characterize the spatial variability of the dune types, sizes, and other morphological properties of the region, making it an interesting case study for this research.

The Skeleton Coast (fig. 3d) dune field contains simple, locally compound, transverse and barchanoid dunes over its 2000 km<sup>2</sup> span according to [17]. The dunes pattern in this region are formed due to onshore winds and surface roughness changes between the dunes and coastal plains. The dune field is roughly aligned with the coast and is characterized with a large slip face in which dunes range from 20m to 80m in height.

Another region represented in the dataset is the Simpson (fig. 3c) dune field in Australia. Much like the Kalahari sands in southern Africa, the Simpson dune fields contains many similar features. The areas are home to lush vegetation, and the dune field follow a mostly simple linear pattern where the dunes tend to be broad crested [13]. According to [38], some of the ridges continue unbroken for up to 200 km, where each crest measures 15m to 38m in height. The spacing between each crest varies depending on the height of the ridges. Areas with larger ridges may have one or two dunes per kilometer, while smaller ridges may have five or six dunes per kilometer. These factor make this area an interesting addition to the dataset because the scale of the images is much larger.

Also present is the Winnemucca Dune Complex (WDC, fig. 3e) found in western United States, in Nevada. The WDC covers an area of roughly 900 km<sup>2</sup> north of Winnemucca, Nevada.

The most common dune type present are stabilized parabolic dunes, but barchans and transverse ridges can also be found scattered throughout the area [15]. In fact, according to [27], the WDC is primarily covered by six crescentic complexes, a large sand sheet, and discontinuous sets of compound barchanbolic-parabolic dune fields. The WDC contains a complex set of repetitive sequences of dunes which varying shapes and scales, which makes it an ideal candidate for this dataset.

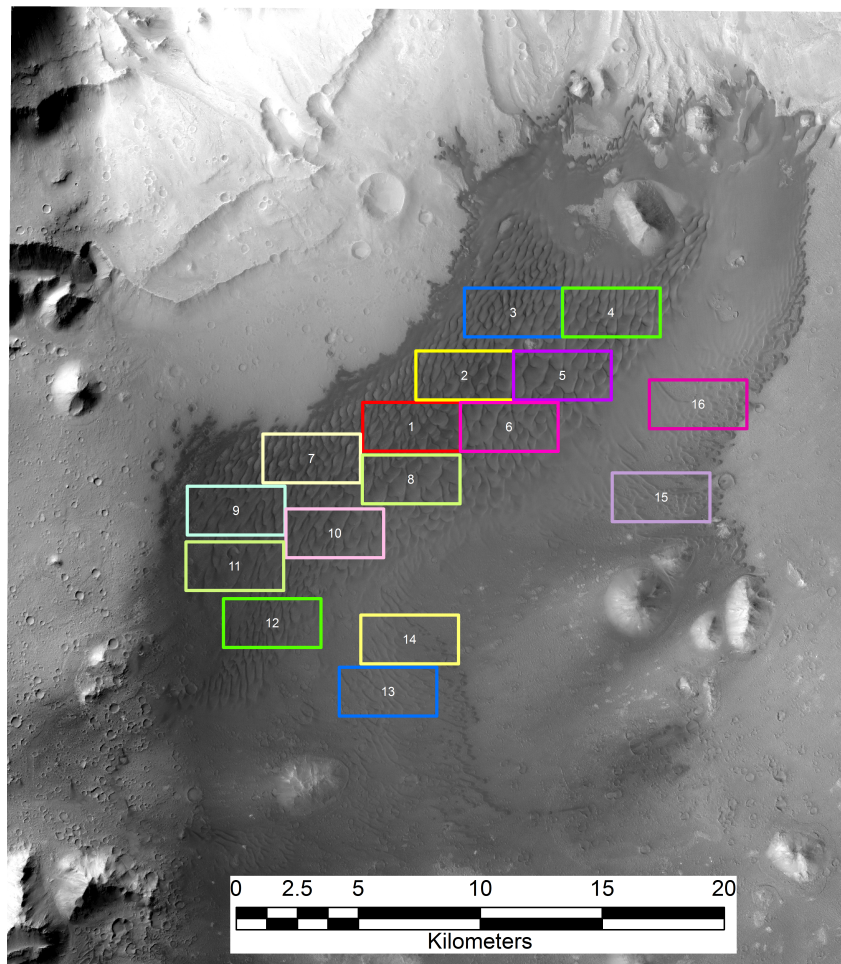
Finally, the last area in the dataset is the White Sands National Monument (fig. 3f), located in the state of New Mexico, USA. This area boasts an interesting pattern of crescentic aeolian dunes which are formed in a systematically similar fashion to wind ripples and subaqueous dunes [32]. There are a wide range of features and properties in the White Sands dune field that merit study, such as described in [32]. These interactions include merging, lateral linking, defect repulsion, bedform repulsion, off-center collision, defect creation and dune splitting. The details of these interactions are outside the scope of this research but crest-line detection may be an essential preliminary step towards extracting those features. Measuring the number of dunes, crest lengths, defect density, dune spacing, and dune height are all done manually by experts in the field. A move towards an automated process would greatly improve research efforts, and would be a helpful tool for scientist in the field.

#### **4.1.2 Mars Dataset**

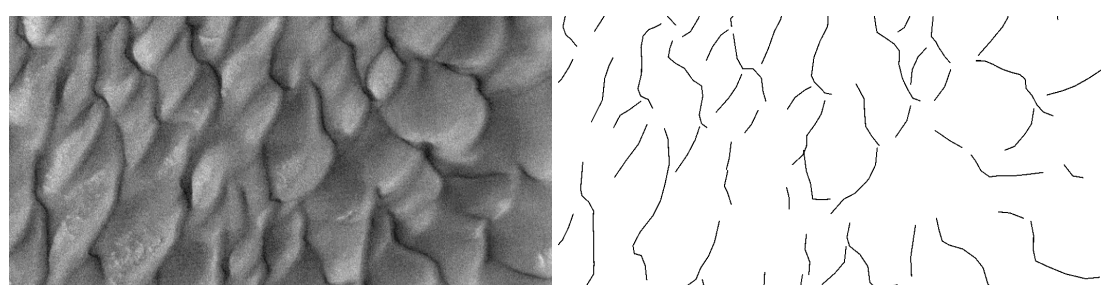
To verify the robustness of this approach, the method was also tested on another dataset which was used in [4]. The dataset provided is from the Ganges chasma on Mars, and includes satellite images, manually labeled crest-lines, and the results of the original author's method. The provided results lay a baseline benchmark for measuring quality and accuracy of crest-line detection algorithms. In order to more easily process the dataset, the Ganges region was split into

sixteen areas of equal size, as shown in Figure 4. The ground truth included was not validated for correctness, the labeled data was used as-is, which may account for some errors (see Sections ?? and ??).

The dataset is essentially a CTX mosaic of the Ganges chasma, which spans an area of 500 km<sup>2</sup>, and includes a wide variety of dune types and morphologies. According to [16], many aeolian features can be found in the Ganges Chasma. Sand sheets, dune fields, unidirectional features such as barchan dunes were all identified within this region. overall structure of the Ganges dune field is a complex set of many diverging dunes, which makes it a challenging and appropriate area for testing this method.



(a)



(b)

Figure 4: Ganges chasma Mars dataset from [4] which includes (4a) 16 regions extracted, (4b) sample image from region 1 with corresponding labeled ground truth

## 5 Conclusion

This is the Conclusion

## References

## References

- [1] A fast two-dimensional median filtering algorithm. *IEEE Transactions on Acoustics, Speech, Signal Processing*, 27(1):13–18, 1979.
- [2] R. Manduchi C. Tomasi. Bilateral filtering for gray and color images. *Proceedings of the 1998 IEEE International Conference on Computer Vision*, 1998.
- [3] Chih-Chiang Tai Yung-Chung Wei Chih-Chung Kao, Liang-Hwei Lee. Extracting the ocean surface feature of non-linear internal solitary waves in modis satellite images. ???????????????, ????????????????
- [4] Maria Barata Lori Fenton Timothy Michaels David Vaz, Pedro Sarmento. Object-based dune analysis: Automated dune mapping and pattern characterization for ganges chasma and gale crater, mars. *Geomorphology*, (250):128–139, 2015.
- [5] Garret P. Duffy and John E. Hughes-Clarke. Application of spatial cross correlation to detection of migration of submarine sand dunes. *Journal of Geophysical Research*, 2005.
- [6] Ryan C. Ewing Gary Kocurek. Aeolian dune field self-organization - implications for the formation of simple versus complex dune-field patterns. *Geomorphology*, 2005.
- [7] Mrinmoy Ghorai and Bhabatosh Chanda. A robust faint line detection and enhancement algorithm for mural images. *Fourth National Conference on Computer Vision, Pattern Recognition, Image Processing and Graphics*, 2013.
- [8] Maheshkumar H. Kolekar G.Lloyds Raja. Illumination normalization for image restoration using modified retinex algorithm. *IEEE ???*, 2012.

- [9] Dian Gong and Gerard Medioni. Probabilistic tensor voting for robust perceptual grouping. ???, 2012.
- [10] Andrew S. Goudie. Desert landforms in namibia - a landsat interpretation.
- [11] Andrew S. Goudie. Namib sand sea: Large dunes in an ancient desert.
- [12] Qiang Chen Guoji Zhang and Quansen Sun. Illumination normalization among multiple remote-sensing images. *IEEE Geoscience and Remote Sensing Letters*, 2014.
- [13] Paul P. Hesse. The australian desert dunefields: formation and evolution in an old, flat, dry continent.
- [14] Jason C. Isaacs and Ross Goroshin. Automated cable tracking in sonar imagery. ???????????????????, ????????????????????
- [15] Steven H. Williams James R. Zimbelman. Eolian dunes and deposits in the western united states as analogs to wind-related features on mars.
- [16] R. A. Beyer L. K. Fenton, T. I. Michaels. Aeolian sediment sources and transport in ganges chasma, mars: Morphology and atmospheric modeling. 2012.
- [17] N. Lancaster. Dunes on the skeleton coast, namibia (south west africa): Geomorphology and grain size relationships. *Earth Surface Processes and Landforms*, 7:575–587, 1982.
- [18] N. Lancaster. Winds and sand movements in the namib sand sea. *Earth Surface Processes and Landforms*, 10:607–â€¢619, 1985.
- [19] N. Lancaster. Development of linear dunes in the southwestern kalahari southern africa. *Journal of Arid Environments*, pages 233–244, 1987.

- [20] Samuel H. Lewis and Aijuan Dong. Detection of breast tumor candidates using marker-controlled watershed segmentation and morphological analysis. *IEEE ???*, 2012.
- [21] Jose Saraiva Lourenco Bandeira, Jorge S. Marques and Pedro Pina. Advances in automated detection of sand dunes on mars. *Earth Surface Processes and Landforms*, 2013.
- [22] David G. Lowe. Distinctive image features from scale-invariant keypoints. *International Journal of Computer Vision*, 2004.
- [23] S. Lewin M.W. Telfer, RM. Fyfe. Automated mapping of linear dunefield morphometric parameters from remotely-sensed data. *Aeolian Research*, 2015.
- [24] B. Triggs N. Dalal. Histograms of oriented gradients for human detection. *CVPR*, pages 886–893, 2005.
- [25] Lei Zhang Paul Bao and Xiaolin Wu. Canny edge detection enhancement by scale multiplication. *IEEE Transaction on Pattern Analysis and Machine Intelligence*, 2005.
- [26] C. Nishan Canagarajah Paul R. Hill and David R. Bull. Image segmentation using a texture gradient based watershed transform. *IEEE Transactions on Image Processing*, 2003.
- [27] Nathaniel Pepe. *The Geomorphology, Eolian Activity, and Petrology of the Winnemucca Dune Complex, Humboldt County, Nevada, USA*. PhD thesis, University of Nevada, Reno.
- [28] R. E. Woods R. C. Gonzalez. *Digital Image Processing*. 2008.
- [29] Jos B.T.M. Roerdink and Arnold Meijster. The watershed transform: Definitions, algorithms and parallelization strategies. *Fundamenta Informaticae*, 2001.

- [30] John Collomosse Rui Hu, Mark Barnard. Gradient field descriptor for sketch based retrieval and localization. *2010 IEEE International Conference on Image Processing*, pages 1025–1028, 2010.
- [31] Alex G. Hayes Ryan C. Ewing, George D. McDonald. Multi-spatial analysis of aeolian dune-field patterns. *Journal of Geomorphology*, 2014.
- [32] Gary A. Kocurek Ryan C. Ewing. Aeolian dune interactions and dune-field pattern formation: White sands dune field, new mexico. *Sedimentology*, 57:1199–1219, 2010.
- [33] Gary Kocurek Ryan C. Ewing, Aymeric-Pierre B. Peyret and Mary Bourke. Dune field pattern formation and recent transporting winds in the olympia undae dune field, north polar region of mars. *Journal of Geophysical Research*, 2010.
- [34] C. Meena S. Malathi, S. Uma Maheswari. Fingerprint pore extraction based on marker controlled watershed segmentation. *IEEE*, 2010.
- [35] Qing Guo Fangmin Dong Shuai Wanh, Shuifa Sun and Chunyan Zhou. Image edge detection based on rotating kernel transformation. *7th International Congress on Image and Signal Processing*, 2014.
- [36] Xiangrong Zhang Shuang Wang, Xuili Ma and Licheng Jiao. Watershed-based textual image segmentation. *International Symposium on Intelligent Signal Processing and Communications Systems*, 2007.
- [37] Jeffrey Brokish Trish Keaton. A level set method for the extraction of roads from multi-spectral imagery. *Applied Imagery Pattern Recognition Workshop*, 2002.
- [38] C. R. Twidale. The simpson desert, central australia. *South African Geographic Journal*, 65:3–17, 1980.

- [39] Wei Zhang Weibin Rong, Zhanjing Li and Lining Sun. An improved canny edge detection algorithm. *IEEE International Conference on Mechatronics and Automation*, 2014.
- [40] Qingbo Geng Xiaobing Wang, Baokui Li. Runway detection and tracking for unmanned aerial vehicle based on an improved canny edge detection algorithm. *4th International Conference on Intelligent Human-Machine Systems and Cybernetics*, 2012.
- [41] Zhigang Jin Yu Cheng and Cunming Hao. Illumination normalization based on 2d gaussian illumination model. *International Conference on Advanced Computer Theory and Engineering (ICACTE)*, 2010.
- [42] Hong Zhang Zhijie Wang. Edge linking using geodesic distance and neighborhood information. *International Conference on Advanced Intelligent Mechatronics*, 2008.